LAWRENCE
LIVERMORE
NATIONAL
LABORATORY

LLNL-CONF-643486

Monte Carlo simulation of neutron noise effects on beam position determination with real and simulated beam images at the National Ignition Facility

A. Awwal, R. Leach, P. Datte, A. Manuel

September 6, 2013

SPIE Optics + Photonics 2013 Conference
San Diego, CA, United States
August 25, 2013 through August 29, 2013

Disclaimer

Monte Carlo simulation of neutron noise effects on beam position determination with real and simulated beam images at the National Ignition Facility

Abdul A. S. Awwal, Richard R. Leach Jr., Philip Datte, and Anastacia Manuel

Integrated Computer Control System, National Ignition Facility
Computational Engineering Division
Lawrence Livermore National Laboratory, Livermore, CA. 94551
E-mail: awwal1@llnl.gov

ABSTRACT

Images obtained through charged coupled device (CCD) cameras in the National Ignition Facility (NIF) are crucial to precise alignment of the 192 laser beams to the NIF target-chamber center (TCC). Cameras in and around the target chamber are increasingly exposed to the effects of neutron radiation as the laser power is increased for high energy fusion experiments. NIF was carefully designed to operate under these conditions. The present work examines the degradation of the measured TCC camera position accuracy resulting from the effects of neutron radiation on the sensor and verifies operation within design specifications. Both synthetic and real beam images are used for measuring position degradation. Monte Carlo simulations based on camera performance models are used to create images with added neutron noise. These models predict neutron induced camera noise based on exposure estimates of the cumulative single-shot fluence in the NIF environment. The neutron induced noise images are used to measure beam positions on a target calculated from the alignment images with the added noise. The effects of this noise are also determined using noise artifacts from real camera images viewing TCC to estimate beam position uncertainty.

Key words: Neutron irradiated CCD, Neutron induced Noise modeling, laser alignment, Monet Carlo simulation, fusion neutron

1. INTRODUCTION

The National Ignition Facility (NIF), operated at the Lawrence Livermore National Laboratory, is 192-beam, 1.8-megajoule, 500-terawatt, ultraviolet laser system designed to demonstrate inertial confinement fusion in a laboratory setting [1]. In preparation for laser fusion and energy gain, as the laser power is ramping up, cameras situated around the target chamber gathering alignment images, are subjected to fusion neutrons generated by laser-target interactions. These neutrons appear as noise in the alignment images, and hence may affect various alignments performed inside the target chamber such as for the beam to target and various other fiducials [2-3]. The objective of the current work is to evaluate the effects of neutron radiation on the alignment performance using Monte Carlo simulation.

The integrated automated control system aligns 192 NIF beams by measuring the beam position using algorithms on images collected by CCD camera and controlling mirrors and other devices to adjust the beam to a desired reference location [4]. Alignment images affected by the neutron noise are the target area beam image (left) and the Chamber center reference system (CCRS) to (target alignment system) TAS images (right). The present study will evaluate the effect of neutron-induced noise on the measured position of the beam from both of these types of images.

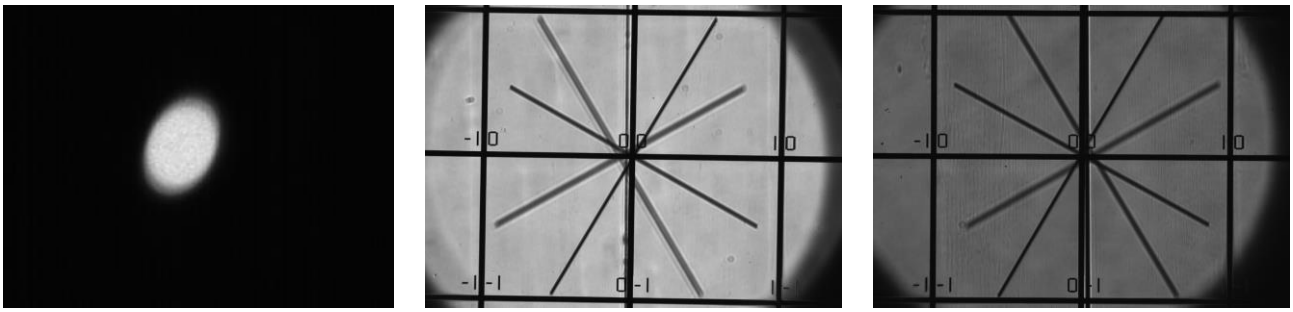

Figure 1: Target area NIF alignment images. The left image is the alignment beam to target and the right two images are the CCRS to TAS image.

2. NOISE SIMULATION

An accurate CCD neutron-induced noise estimation was first established at an experimental accelerator facility designed to produce 14 MeV neutrons. An accurate measurement of the neutron-induced noise was performed for different fluence levels up to $1x10^{10}$ (n/cm^2) on the sensor surface. The results from these measurements were then scaled to the higher fluence levels expected on NIF. The noise models do not include induced noise associated with gamma radiation. The noise model provides one instance of the noise for a neutron fluence level for a particular alignment camera. One thousand instances of this noise model are created using Monte Carlo technique.

Fluence maps for the target bay and target chamber describe the estimated fluence levels at various locations based on a shot of known yield. Knowledge of the CCD detector plane location in the target area provides an estimate of the expected fluence level for the sensor. The cumulative neutron yield discussed here is the number of neutrons generated at the target chamber center into 4π steradians for several shots. The target area beam CCD sensors, when retracted during a shot, are located outside the five meter distance from target chamber center. The fluence maps, arbitrarily scaled to a yield shot of 10^{15} (neutrons) indicate a fluence level of $6x10^8$ (neutrons/cm^2) at the sensor. The CCD noise model matches the statistical distribution of real neutron-affected pixels at the physical camera location in the target bay [4-6].

When a neutron hits a CCD pixel, there is a small probability that it causes permanent increased dark current (noise) in that pixel. The affected pixel may have noise slightly over the background, be fully saturated, or anything in between. Background images are captured before and after shots of the NIF laser to measure the pixel noise. We express the number of neutron-affected pixels statistically as a reversed-sum histogram curve, as shown in Figure 2, in order to quantify the number of affected pixels through the whole range of gray scale levels. The curve is essentially a modified cumulative distribution function (CDF) that ranges up to 100% of the pixels on the y-axis that are greater than the pixel intensity values on the x-axis (0 to 4095 for a 12-bit camera).

In a standard CDF, $F_x(x) = P(X \leq x)$, the curve represents the probability that a random variable X takes a value less than or equal to x. In the reversed-sum histogram $F_x(x) = P(X \geq x)$, the curve represents the number of pixels with intensity values greater than or equal to x. Thus, on the curve shown in Figure 2, a point on the lower knee represents the percentage (between 0.001% and 0.01%) of pixels whose intensity value is 3000 or higher. The knees on the curves show the number of damaged pixels (noisy pixels) with respect to the pixels that did not get damaged. A properly working CCD will have a single knee (at the top) and an almost vertical drop.

The reversed-sum histogram curves in Figure 2 were obtained from background images for one of the four TAS (Target Alignment Sensor) cameras used in target area beam alignment from December 16, 2010 through February 2, 2011 (dates are indicated by YYMMDD in the legend). Before February 1, the shots on NIF did not generate considerable neutron yield. As a result, before 110202, the cumulative neutron-induced effect is consistent and the curves superimpose on each-other. After a yield shot of 1.2×10^{14} neutrons on February 1st, the background image collected the next day shows an increase in number of pixels with elevated intensity values between the two knees. The fluence models show that the neutron fluence at the sensor was approximately ~$1x10^8$ (n/cm^2) for this yield shot.

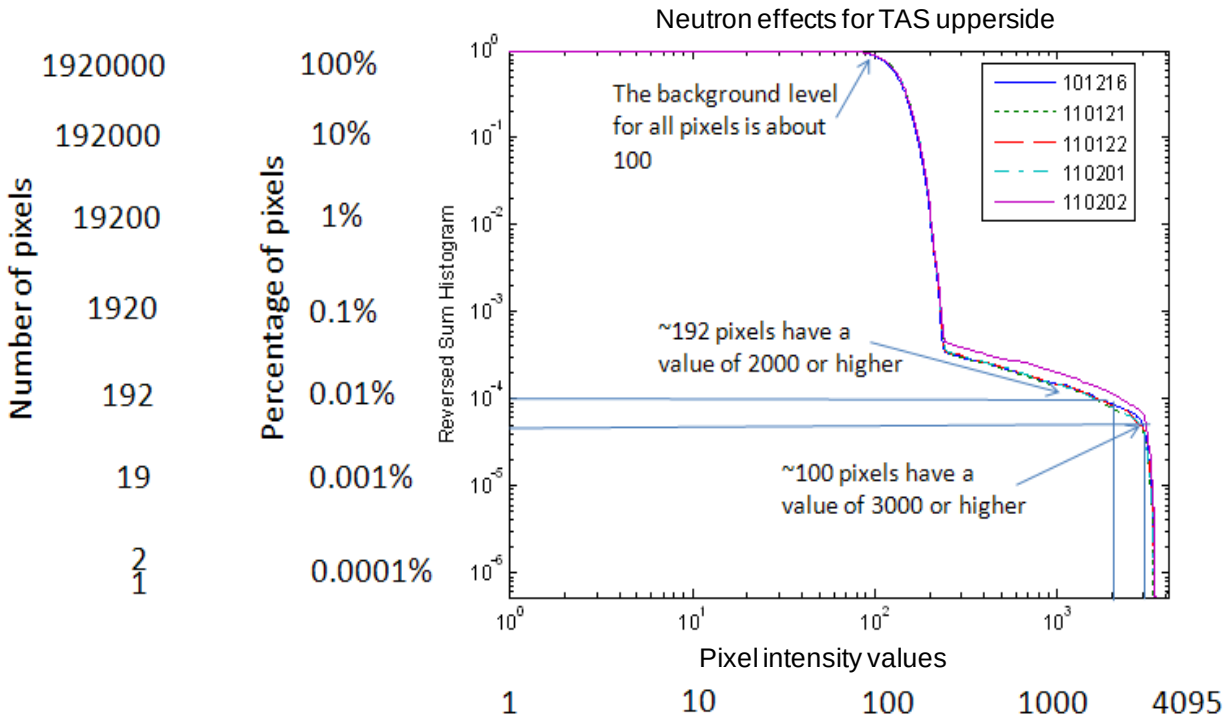

Figure 2: A reversed-sum histogram curve for one of the TAS (Target Alignment Sensor) cameras. This 12-bit camera has 1200×1600 pixels (1,920,000 total pixels) and a maximum pixel intensity value of 4095. The data collected between 12/16/10 and 2/1/11 have no change in the curve shape because there is low neutron yield at this time. After a shot of 1.2×10^{14} neutrons on 2/1/11, the background image collected the next day shows an increased number of pixels with elevated intensity values. (The legend lists the date of the data collection in YYMMDD format.)

As the CCD pixels are exposed to higher neutron yields, an increasing number of pixels will have increasingly elevated intensity values and reversed-sum histogram curve shifts upwards. The amount that the curve shifts can be predicted based on a linear model from the curves dating back to the first neutron-yield shot and from offline measurements taken at the accelerator facility. A statistical noise model was then developed based on the increased pixel noise measured after each shot. The increased noise is then scaled to the shot yield where predictions can then determine the expected noise content in the image. Figure 3 is an example of the predicted neutron-induced noise expected for cumulative neutron yields of 10^{15}, 10^{16}, 10^{17} and 10^{18} neutrons. Note that in this model the dynamic range has not been limited to the camera bit-length. However, for simulating a neutron noise induced image, when the noise is added to the real image, the sum intensity is limited to the value allowed in the camera.

Given a simulated reversed-sum histogram for a specific neutron yield, a neutron-background image can be generated by randomly assigning pixels in the image to have the appropriate noise background levels as dictated by the by the reverse-sum histogram noise curves as shown in Figure 3. The simulated neutron-background images after a neutron yield shot contains all noise expected in the image including the increased pixel counts due to the neutrons and all the other regular noise sources (i.e. dark current, read noise, etc., which create a background of about 100 counts for the particular camera setting including gain and integration time). Figure 4 shows four of the 4000 instances of modeled neutron noise representing all noise levels. Each noise level whose characteristic is depicted in the reverse sum histogram (reversely integrated probability density function), 1000 separate instance of randomly allocated noise images are created as described in Fig. 5. To generate a realistic target area beam image with neutron induced-noise, the TAS image is added to one of the 1000 noise images. The 4000 noise added images are then processed using image processing algorithm discussed in the next section. Our previous study involved four noise images with 192 beams [8], which is an example of variation of signal level and type instead of just the noise.

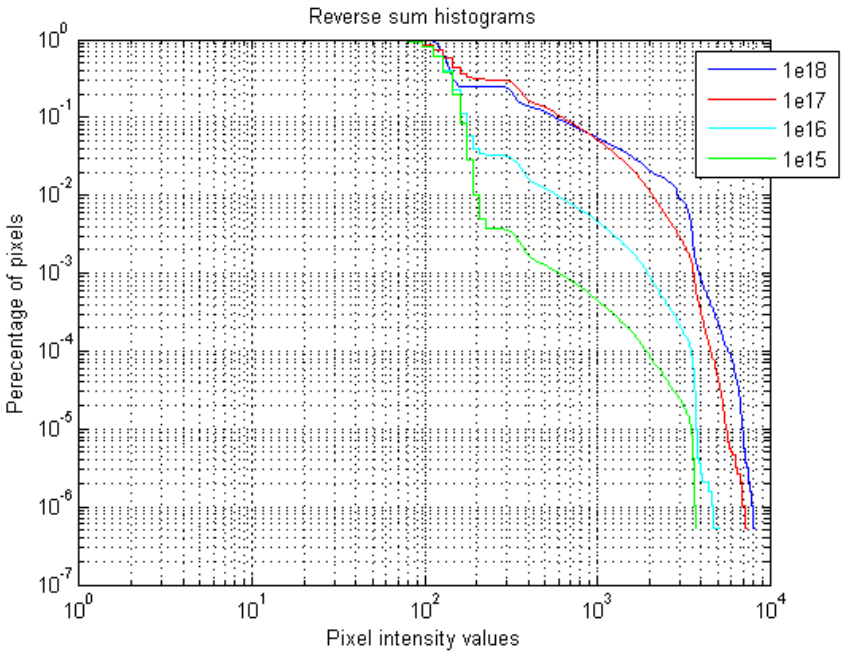

Figure 3: Predicted reversed-sum histograms for TAS camera pixel values scaled for cumulative neutron yields between 10^{15} and 10^{18} neutrons at the target chamber center which was used for the simulation.

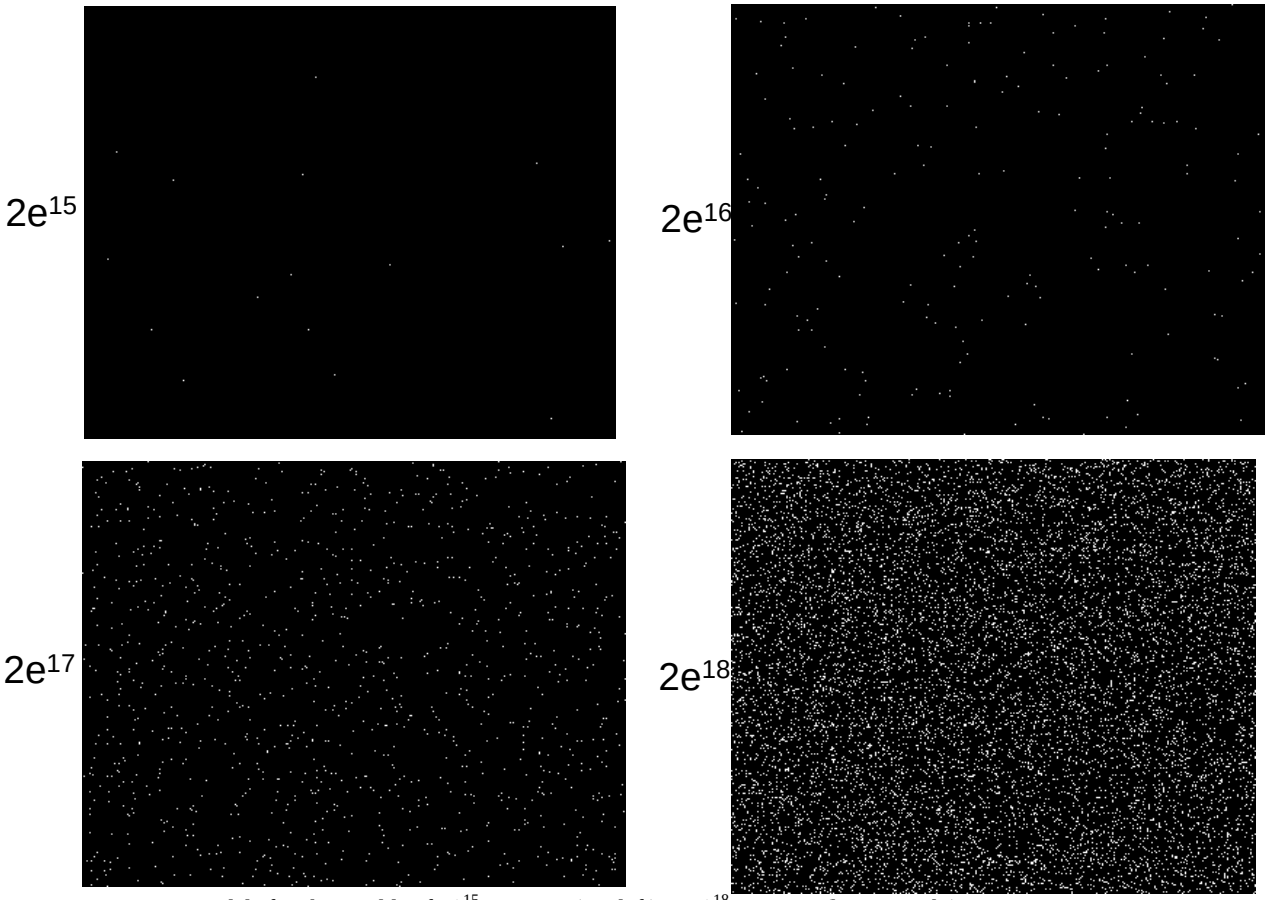

Figure 4: Noise models for shot-yields of 10^{15} neutrons (top left) to 10^{18} neutrons (bottom right).

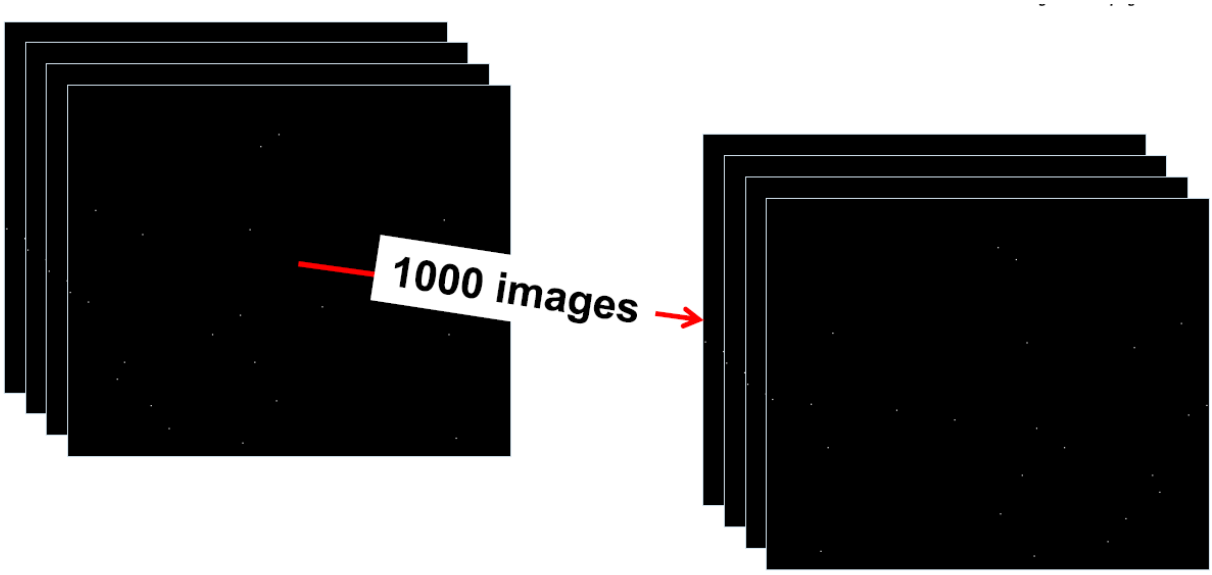

Figure 5: Noise pixels positions were permuted to random pixel positions in each generated image

3. MONTE CARLO EXPERIMENTS

Two types of images are analyzed for evaluating the effect of neutron noise on beam alignment, the first is the beam to tas image, and the second one is the CCRS to tas images. The algorithms used and results obtained are described next.

3.1 Beam to TAS position estimation

The position of the "beam to tas" image is estimated using weighted centroid of the bright region above the background level. In the background subtraction stage, a value proportional to the noise floor plus a fraction of the image maximum is subtracted from the beam image. One of the advantages of the subtraction at a slightly higher level than the mean background is the removal of ghost sidelobes that propagate with the beam and affect the centroid result drastically. After the noise subtraction, the largest size of connected region above noise level is chosen for estimating the weighted centroid. The block diagram of the image processing steps is shown in Figure 6.

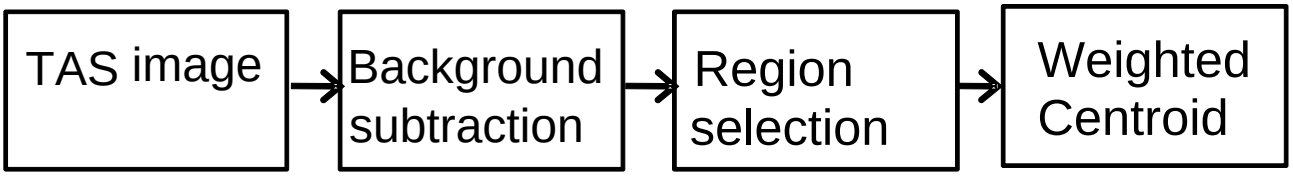

Figure 6: Block diagram of the centroiding approach

In order to have a better control of the experiment in addition to a real NIF beam, an ideal Gaussian beam is analyzed. The algorithm estimates the position of target area beam images added with one thousand instances of neutron noise images. The set of 1000 images with a specific noise levels leads to 1000 different position estimate from which the statistical deviation of the centroid estimate is calculated. The deviation of the noise estimates from noise- free case is plotted in a scatter plot shown in Fig. 7. The standard deviation of these estimates is around 0.11 pixels for the 10^{18} noise level. The Table 1 depicts the corresponding values for all noise levels.

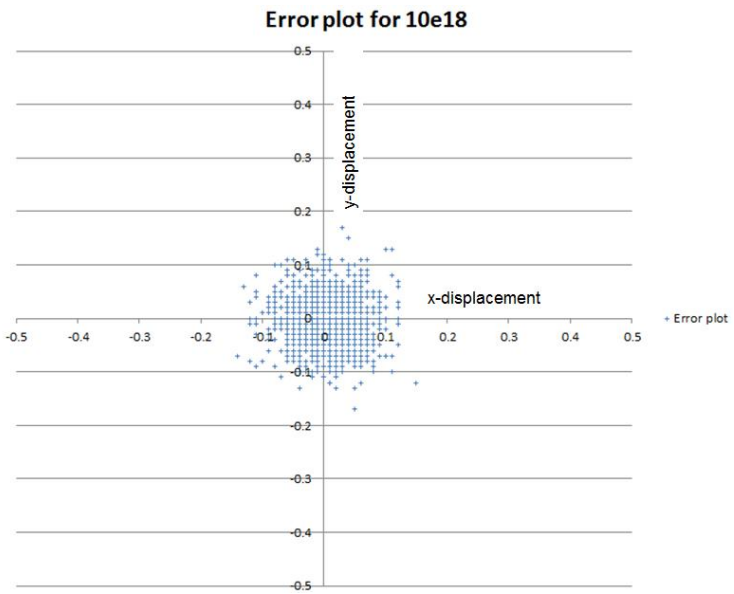

Figure 7: Current algorithm on synthetic image deviation of centroid for a 10^{18} neutron yield (highlighted in Table 1).

Algorithm Modification: One of the limitations of the above algorithm is its sensitivity to the image maxima. If the value of the noise maxima is corrupted by the neutron noise, the corresponding threshold and hence the centroid value may be affected. The centroiding algorithm was modified as explained in the block diagram of Figure 8. These steps in the algorithm identify the noise locations and filter them, and the other step modifies the image maximum detection algorithm so that the image maximum is not affected by the isolated neutron noise. First, the difference between a median filtered image and image with noise will be calculated to identify the position of the neutron-induced noise. When the difference is above a threshold (of 300), those pixels were identified as noisy pixels. The values of only those pixels were changed to the median value of the image at that location. Image values at all the other pixel locations remained unchanged. In addition, the image maximum went through several additional tests. The first criterion was to ensure that the maximum is chosen from only the bright connected region, and not an isolated pixel outside the beam. Then, a neighborhood check was performed to ensure the maximum and the neighboring pixels are similar in magnitude.

Table 1. Synthetic image results

Old Algorithm (synthetic image)

Noise	X-range	Y-range	x-sigma	y-sigma	radial
1e15	0.16	0.140	0.020894	0.021658	0.0300093
1e16	0.137	0.140	0.02265	0.02268	0.03205
1e17	0.1779	0.19567	0.030033	0.0307464	0.04298
1e18	0.8333	0.723206	0.11072	0.111616	0.15722

Current Algorithm (synthetic image)

Noise	X-range	Y-range	x-sigma	y-sigma	radial
1e15	0.13049	0.13256	0.019267	0.019735	0.0275806
1e16	0.1377	0.13708	0.020266	0.020616	0.0289
1e17	0.16	0.15	0.023214	0.023213	0.03213
1e18	0.29	0.34	0.045789	0.048856	0.066959

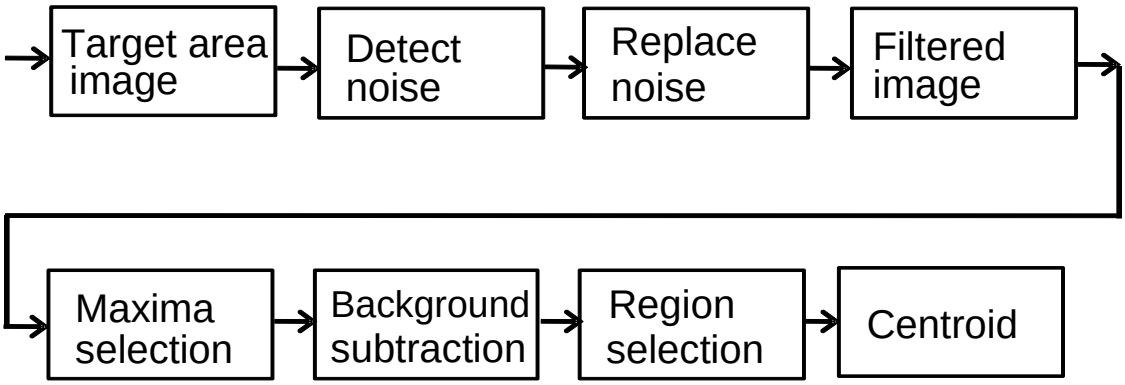

Figure 8: Block diagram of the current centroiding approach with noise filtering.

When this modified algorithm is applied to the same dataset with an ideal Gaussian beam the deviation is improved for all the noise levels, while the improvement is significant for noise levels above 10^{16}. At lower noise level, the improvement is less because the filtering is applied only on handful of pixels. For the real beam, the magnitude of the deviation is less than those of the ideal Gaussian beam as shown in Table 2. Fig. 9 and 10 depicts both ideal and real beam results graphically. It may be noted that at higher noise levels, the rate of increase of the noise deviation is reduced by the introduction of the new limited filtering algorithm.

Table 2. Comparison of deviations with old and new algorithm using real NIF beam image

Old Algorithm (real image)

Noise	X-range	Y-range	x-sigma	y-sigma	radial
1e15	0.0512085	0.057251	0.0086354	0.0089100	0.0124080
1e16	0.048645	0.080078	0.0071195	0.0107261	0.0128739
1e17	0.087524	0.118835	0.0139912	0.0199774	0.0243896
1e18	0.291077	0.390442	0.0441285	0.0609	0.075207

Current Algorithm (real image)

Noise	X-range	Y-range	x-sigma	y-sigma	radial
1e15	0.0385132	0.0501099	0.00598618	0.00865598	0.0105243
1e16	0.0437012	0.0560303	0.00628195	0.00848364	0.0105563
1e17	0.0641479	0.072015	0.00924912	0.0114217	0.0146970
1e18	0.160339	0.210754	0.025359	0.032926	0.041559

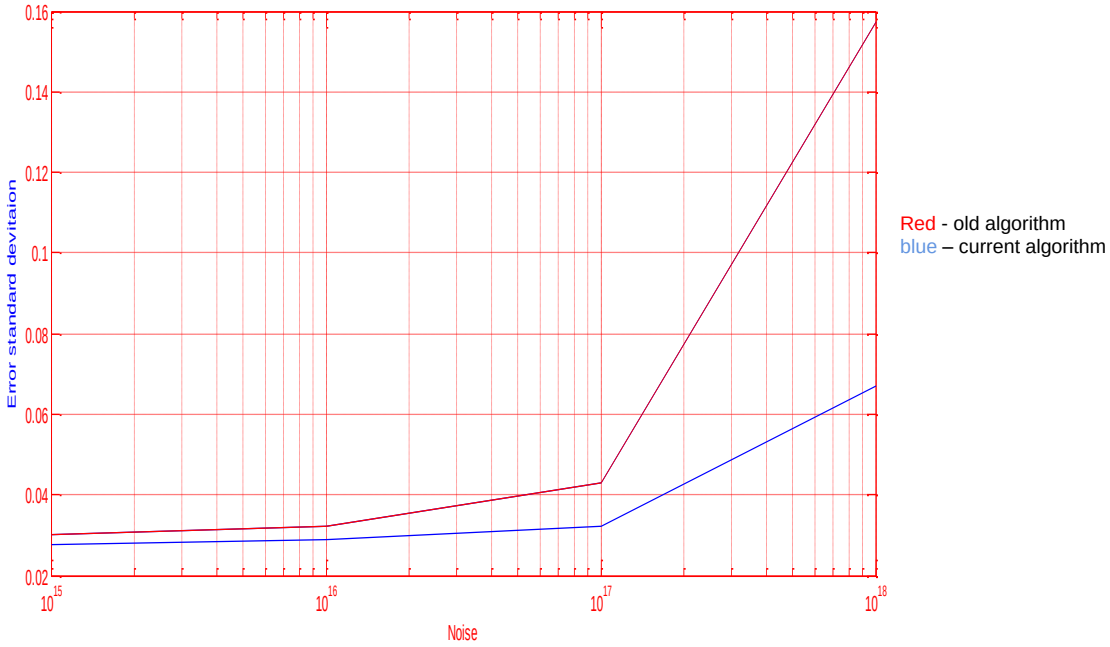

Figure 9: Synthetic image results, comparison of old and current algorithm in terms of standard deviation the beam centroid position with a noise distribution for a yield of $1e^{15}$ to $1e^{18}$ neutrons using Monte Carlo simulation of 4000 images.

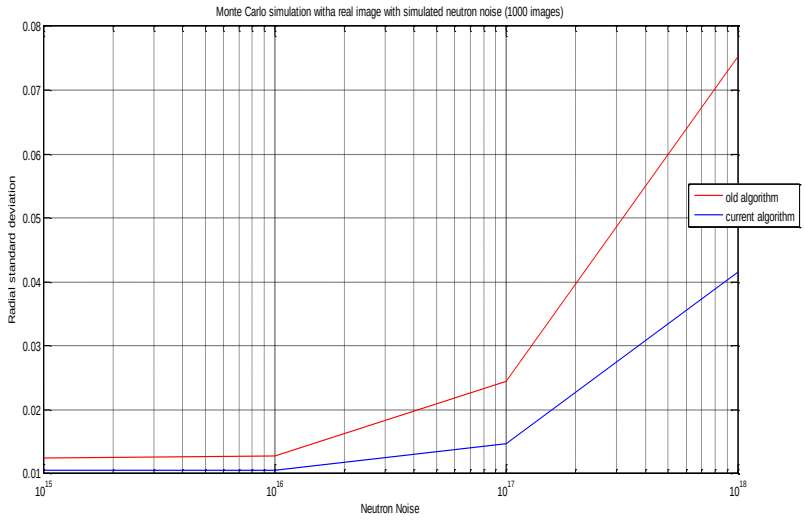

Figure 10: Real NIF beam results, comparison of old and current algorithm in terms of standard deviation the beam centroid position with a noise distribution for a yield of $1e^{15}$ to $1e^{18}$ neutrons using Monte Carlo simulation of 4000 images.

3.2 CCRS TO TAS position estimation

The centering position of the CCRS to TAS is estimated from reference lines and markings in images from two cameras in the target alignment system. The cameras are positioned orthogonal to each other as seen in Figure 11.

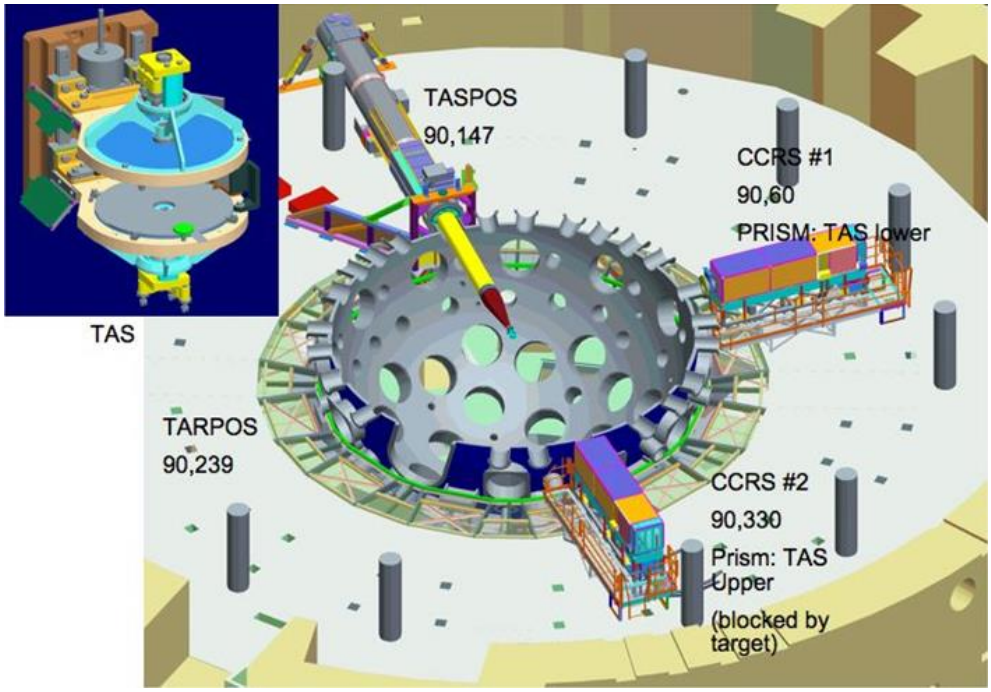

Figure 11: Target alignment system (TAS) is inserted and centered using two cameras in the chamber center reference system (CCRS). CCRS #1 and CCRS #2 which are positioned orthogonal from each other and collect images of the target for processing to achieve the proper target centering alignment.

One image from each CCRS camera is taken to determine the centering position of the target. Both images have a grid pattern whose center is the reference in the image. The center of two of the other lines in the images makes up a reticule. The grid and reticule for both cameras is shown in Figure 12. The reticule center location relative to the grid center indicates the target centering position. When the reticule center is positioned directly over the grid center, the target is optimally centered.

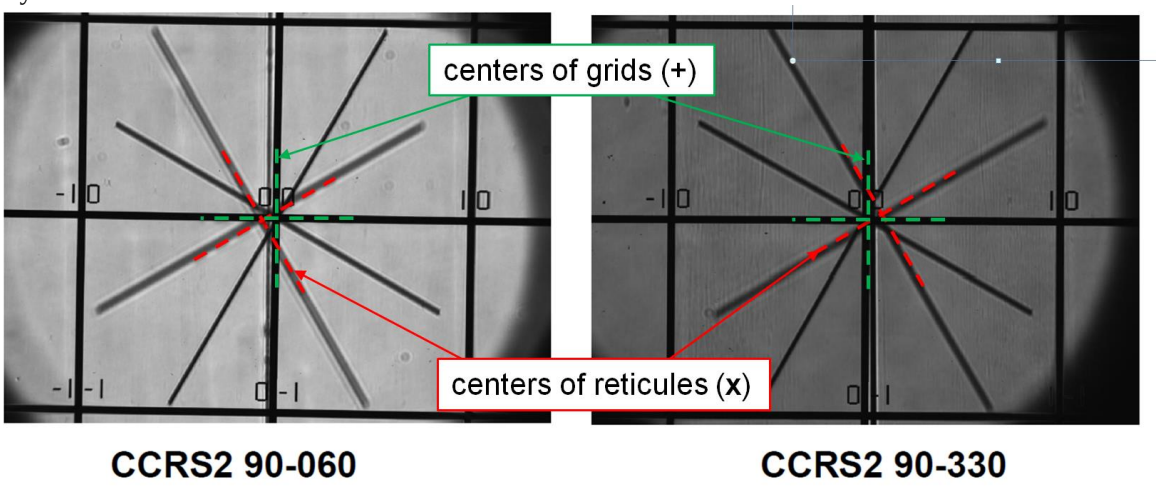

Figure 12: Grid and reticule patterns in CCRS #1 and CCRS #2 camera images. Positioning the reticule center directly over the grid center indicates correct centering of the target.

The grid and reticule centers are made up of two lines each and are found by locating and estimating the position of each line and their resulting intersection using the image processing algorithm shown in the block diagram in Figure 13.

To estimate a line position in the image, the image is rotated to position the target line vertically in the image. The image is then segmented into a set of horizontal bands. Each band is averaged to form a set of intensity vectors that consist of the mean intensity in each band. The vectors are then processed to locate the maximum change in contrast, both light to dark and dark to light. These changes represent the edges of the target line and their mean is stored as the center of the target line for each band. This process results in a series of points from which outliers are removed. A linear fit is performed using the final set of points. The process is repeated for the second line in the grid or reticule pattern. The intersection of the resulting two lines is then used as the grid or reticule position.

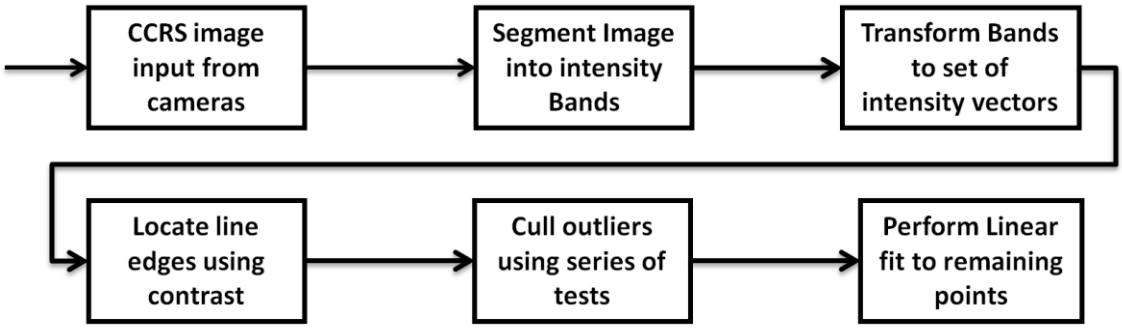

Figure 13: Block diagram of the image processing for estimating the centers of the grid and the reticule for the TAS to CCRS

Next the CCRS images are subjected to Monte Carlo simulation. A typical NIF CCRS image for each camera was chosen and added with one thousand instances of neutron noise images. The resulting set of 1000 images was processed with the above algorithm. This produced 1000 different x and y position estimates from which the statistical deviation is calculated. Error was calculated using the original images position as compared to each of the 1000 images with the random neutron nose added. The average standard deviation of the grid and the reticule estimates was around 0.12 pixels for the 10^{18} added neutron nose for the CCRS 090 030 camera. The average standard deviation of the grid and the reticule estimates was around 0.16 pixels for the 10^{18} added neutron noise for the CCRS 090 060 camera. The table and figures below depict the corresponding values for all noise levels.

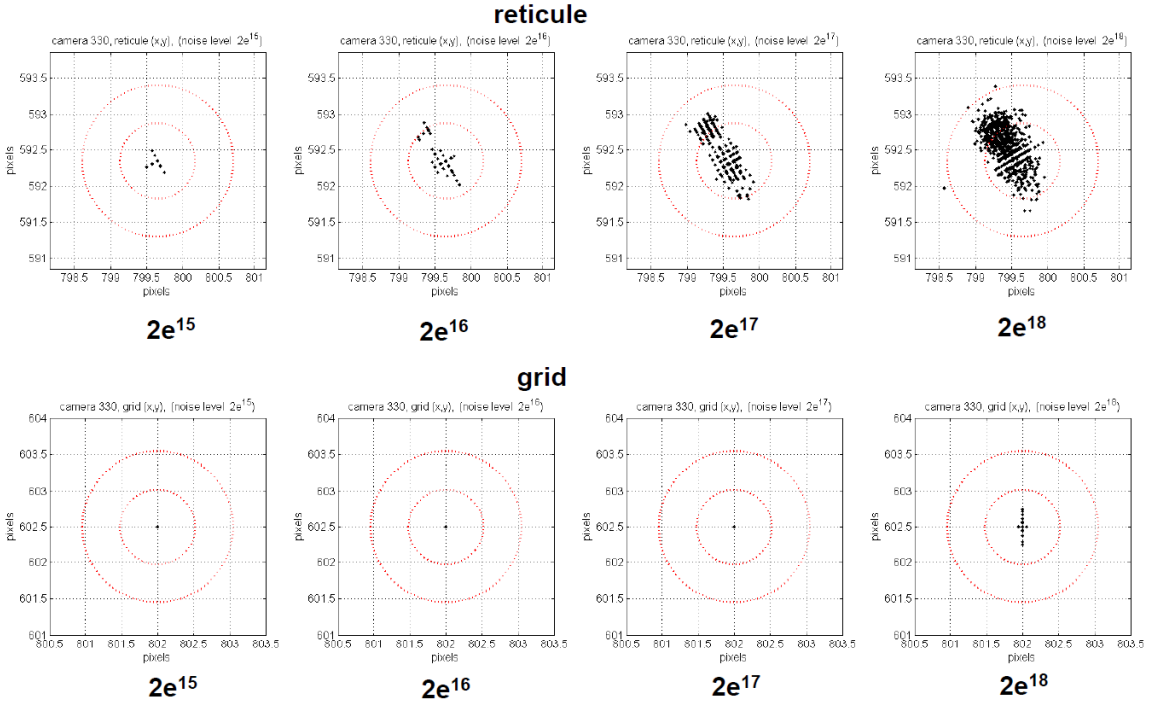

Figure 14: CCRS to tas images position error for reticule and grid scatter plot

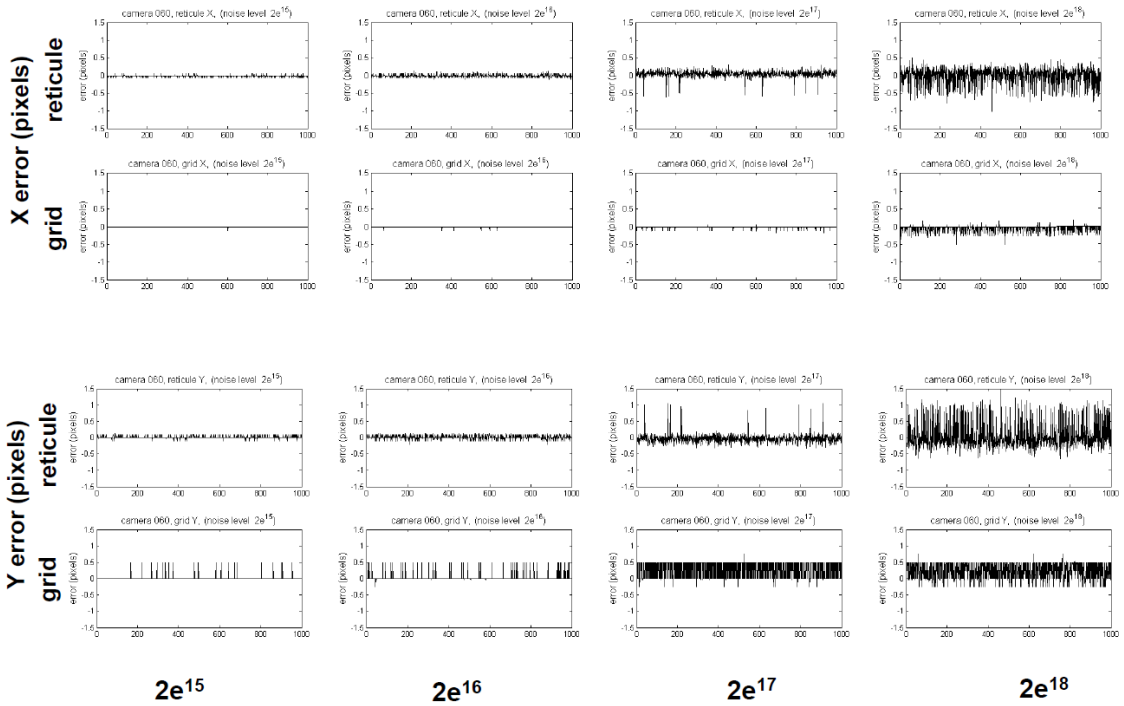

Figure 15: CCRS to tas images position error for reticule and grid for 1000 images at each noise level

Table 3. CCRS to tas images position error for reticule and grid

CCRS 90-330								
Neutron	reticule position error				grid position error			
damage	x		y		x		y	
level	(pixels)	(pixels)	(pixels)	(pixels)	(pixels)	(pixels)	(pixels)	(pixels)
	mean	stddev	mean	stddev	mean	stddev	mean	stddev
2.E+15	-0.0012	0.0125	-0.0006	0.0123	0.0000	0.0000	0.0000	0.0000
2.E+16	-0.0181	0.0578	0.0064	0.0833	0.0000	0.0000	0.0000	0.0000
2.E+17	-0.1228	0.1430	0.0588	0.2258	0.0000	0.0000	0.0000	0.0000
2.E+18	-0.2312	0.1817	0.2081	0.2581	-0.0002	0.0081	0.0027	0.0270

CCRS 90-360								
Neutron	reticule position error				grid position error			
damage	x		y		x		y	
level	(pixels)	(pixels)	(pixels)	(pixels)	(pixels)	(pixels)	(pixels)	(pixels)
	mean	stddev	mean	stddev	mean	stddev	mean	stddev
2.E+15	-0.0052	0.0202	0.0102	0.0332	-0.0001	0.0035	0.0105	0.0717
2.E+16	-0.0010	0.0348	0.0141	0.0521	-0.0008	0.0093	0.0251	0.1104
2.E+17	0.0461	0.0904	-0.0283	0.1367	-0.0043	0.0224	0.2852	0.2503
2.E+18	-0.0093	0.2407	0.0368	0.3959	-0.0412	0.0846	0.2341	0.2479

4. CONCLUSIONS

In this paper, Monte Carlo simulation is used to quantify the effects of neutron induced noise on estimation of beam location. The noise model developed to simulate the effect of neutron-induced noise on an image. It was found that with old algorithm the deviation increase exponentially at higher noise level, the rate of change of deviation is significantly reduced with the modified algorithm. One way to expand this study is to include all 192 beam images with 4000 noise images. Classifying the images by intensity parametric set of curves may be derived. Alternate filtering [9] technique may be explored for eliminating the neutron noise effects. With the CCRS to TAS images, the effects of the Monte Carlo added neutron noise were minimal for the images processed, however, further studies are needed to examine worst-case scenarios where neutron effects fall in critical measurement regions in the images.

ACKNOWLEDGEMENT

This work performed under the auspices of the U.S. Department of Energy by Lawrence Livermore National Laboratory under Contract DE-AC52-07NA27344.

REFERENCES

[1] Special issue of Physics of Plasmas on "Plans for the National Ignition campaign (NIC) on the National Ignition Facility (NIF): On the threshold of initiating ignition experiments", guest edited by John Lindl and Edward I. Moses, 5, (2011); see also p. 050901-1 for an overview editorial.

[2] S. C. Burkhart, E. Bliss, D. Kalantar, R. Lowe-Webb, T. McCarville, D. Nelson, … K. Wilhelmsen, "National Ignition Facility system alignment," *Applied Optics, 50*(8), 1136-57 (2011).

[3] K. Wilhelmsen, A. Awwal, W. Ferguson, B Horowitz, V. Miller Kamm, C. Reynolds, "Automatic Alignment System For The National Ignition Facility", Proceedings of 2007 International Conference on Accelerator and Large Experimental Control Systems (ICALEPCS07), 486-490, Knoxville, Tennessee (2007).

[4] C. Hagmann, J. Ayers, P. M. Bell, et al., "Radiation induced noise in x-ray imagers for high-yield inertial confinement fusion experiments," G. P. Grim, and R. C. Schirato edited, Penetrating Radiation Systems And Applications XII, Proc. SPIE 8144, 814408 (2011).

[5] J. E. Brau, O. Igonkina, C. T. Potter, N. B. Sinev, "Investigation of radiation damage effects in neutron irradiated CCD," Nucl. Instr. and Methods Phys. Res. A 549, 117–121 (2005).

[6] A. M. Chugg, R. Jones, M. J. Moutrie, and P. R. Truscott, "Analyses of Images of Neutron Interactions and Single Particle Displacement Damage in CCD Arrays," IEEE Trans. Nucl. Sci., 51, 3579 (2004).

[7] R. Taniguchi, R. Sasaki, S. Okuda, Ken-Ichi Okamoto, Y. Ogawa, T. Tsujimoto, "Noise characteristics of neutron images obtained by cooled CCD device," Nucl. Instr. Meth. Phys. Res. A 605, 85–90 (2009).

[8] A. A. S. Awwal, A. Manuel, P. Datte, M. Eckart, M. Jackson, S. Azevedo, S. Burkhart, "Effects on beam alignment due to neutron-irradiated CCD images at the National Ignition Facility," Proceedings SPIE 8134: Optics and Photonics for Information Processing V, Khan M. Iftekharuddin; Abdul Ahad Sami Awwal, Editors, 81340J (2011).

[9] H. Li, B. Schillinger, E. Calzada, et al., "An adaptive algorithm for gamma spots removal in CCD-based neutron radiography and tomography," Nucl. Instr. Meth. In Phys. Res. A-Accel. Spec. Det. Assoc. Equip., 564(1), 405-413 (2006).